Study on active wheelset steering from the perspective of wheel wear evolution

Authors: Bin Fu[1], Saeed Hossein Nia[2], Sebastian Stichel[2], Stefano Bruni[1]*

1 Dipartimento di Meccanica, Politecnico di Milano, Milano, 20156, Italy

2 Division of Rail Vehicles, KTH Royal Institute of Technology, Stockholm, 10044, Sweden

bin.fu@polimi.it

Abstract: Active wheelset steering promises an attractive cost-benefit ratio and is highly likely to be implemented in the future. Previous studies investigated the steering effect simply through a wear index like wear number. However, a wear index cannot predict how much the material removal on wheels can be reduced and it is unable to reveal the wear pattern. This paper builds an iterative wear model to predict wheel wear evaluation under the presence of an active steering system. Three active steering schemes are proposed, and they are compared in terms of wheel wear evolution. To quantify the steering effectiveness, two factors are created to respectively evaluate economic impacts and satisfaction of three steering schemes. Finally, a simplified method based on traditional wear indices is compared with the established iterative wear calculation method to examine the applicability and tolerance of the simplified method.

Key words*: wear evolution, active steering, control scheme, radial control, effectiveness*

1 Introduction and motivation

Active suspension, as a general concept, is a mixture of many active-controlled technologies in suspension, which has been drawing attention in railway engineering since the 1970s [1] but still has limited application in real service, although huge potential benefits of different active suspension technologies have been demonstrated by numerical and experimental studies [2–4]. Among various active suspension technologies, active wheelset steering is one of the most promising technologies to be extensively implemented in near future.

The implementation of new active suspension technologies imposes two key issues: The possible safety risk and the cost-benefit ratio. The safety issue of active steering schemes for a bogie vehicle has been studied and solutions to guaranteeing the safety and reliability have been proposed, for instance by introducing backup or redundant structures [5]. Regarding the cost-benefit ratio, active steering has an attractive performance [6]. The wear of wheel and rail in small-radius curves can

be significantly reduced [7,8] and Rolling Contact Fatigue (RCF) of the rail can be alleviated [9]. Therefore, a large amount of maintenance cost on wheel and rail is to be saved.

In many previous numerical studies on active steering, the improvement of wear on wheel surface is demonstrated by observing the reduction of the wear number, the longitudinal creep force or some other indices in curves [10,11]. These simulation results cannot illustrate, however, the extent to which wear can be reduced in real operation because the effect of active control on the evolution of wheel profiles due to wear is not considered. Therefore, it is meaningful to predict the wear evolution of the wheel in representative operation conditions. In this study, for the first time, we explore the wear evolution of wheel profiles with active steering technology, which enables a deep understanding of the benefits of this technology. Furthermore, we can visually and quantitatively evaluate the wear distribution over the whole wheel profile, either on wheel flange or wheel tread, which in turn can help to identify potential safety issues in terms of instability and derailment.

Besides the above-mentioned research motivations, this paper aims at facilitating the understanding of different control schemes that might be applied in active steering in future. Previous studies have proposed the perfect control scheme for active steering, but this scheme requires that either the longitudinal creep forces or the lateral displacements of the wheelsets and wheel / rail conicities are measured or estimated in real time [4,8]. This poses significant measurement challenges and the effectiveness of the steering scheme could be impaired by large measuring /estimation errors. Radial control is also proposed, i.e. to steer the wheelset into the radial position in curves [4,5]. This control scheme has shown satisfactory results and is much easier to implement as it only involves the estimation of track curvature and the measure of the yaw rotation of the wheelsets. The principles of radial and perfect steering are fully explained in Section 2.3 and the comparison of these two control concepts is performed in this paper.

The paper is organized as follows. In Section 2, the vehicle dynamics model and actuator dynamics model are briefly introduced. Then the three steering control schemes are explained in detail. Section 3 introduces the wheel wear calculation method and case studies are performed for the vehicle with passive suspension. The wheel wear evolution with steering schemes is studied in Section 4. In this section, the steering schemes introduced in Section 2 are compared, and the influence of track layout is analyzed. In Section 5 a commonly used simplified method is compared with iterative wear calculation method. The paper ends with a discussion of results obtained and conclusions in Section 6.

2 Model of vehicle and active steering system

2.1 Multi-body model of vehicle

The dynamics model of the rail vehicle can be seen as an integration of a passive vehicle model and an active steering system. The passive vehicle model is built in SIMPACK based on a real inter-city trailer vehicle with one car-body, two bogies and four wheelsets, having a targeted maximum service speed of 160km/h. In passive primary suspension, coil springs at the top of the axle-boxes carry the vertical load and provide a small part of the yaw and lateral primary stiffness, while the swing arm with rubber bushings mounted between the axle-box and bogie side beam transfers the longitudinal force and provides the main part of the yaw stiffness. Between the car-body and the bogies, air springs are implemented to provide soft stiffness. Lateral and vertical dampers are mounted to serve suitable damping for ride comfort. Two yaw dampers are arranged to guarantee the stability. The mass properties and passive suspension parameters were examined and modified by a group of experts in the project RUN2RAIL to make the model representative.

The mechanical structure of active steering is to replace the passive swing arm with an actuator at each side of the wheelset. The longitudinal stiffness of coil springs at top of the axle-box should be kept small to avoid that it works too much against the actuator force in curves. Track irregularities considered in this work are measured from a real track operated at speeds up to 160km/h. Irregularity components consisting of longitudinal level, lateral level, cross level and gauge variation are all considered.

2.2 Model of active steering actuation system

The active steering actuation here adopts a Hydraulic-Servo Actuator (HSA) system which is a mature actuator technology applied in industry so far [12,13]. Electro-Hydrostatic Actuator (EHA) is the other promising technology for active steering. However, considering that the working frequency of active steering is normally under 2Hz and the dynamic behaviors of HSA and EHA are negligible based on the two available models [14], we implement an HSA model in this work.

The circuit of the HSA model is illustrated by the schematic diagram in Figure 1. It mainly consists of a double-acting hydraulic cylinder, servo-valve, standby valve, hydraulic pipeline and centralized motor and pump. The motor and pump pressurize constant high-pressure and low-pressure hydraulic oil in two branches of the pipeline network shown in red and blue colours respectively. Oil flow in the chambers of the cylinder is controlled by a ‘3-position 4-way’ servo-valve in which the movement of the spool is proportional to the input signal and thereby the opening area of orifice and path of hydraulic oil are controlled. A Proportional + Integral (PI) controller is

introduced to follow the referenced displacement of the cylinder. The detailed explanation of this circuit and its parameter settings can be found in reference [14].

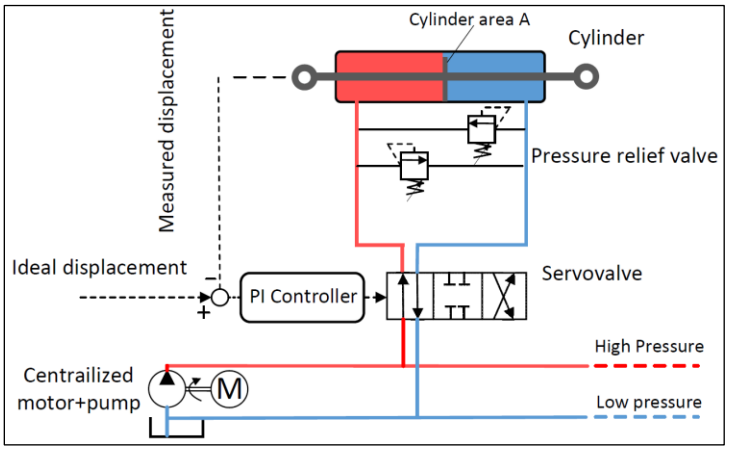

Figure 1 Schematic diagram of HSA circuit

The HSA model is realized in SIMULINK, and co-simulation between SIMPACK and SIMULINK is adopted to integrate the vehicle model and the actuator model. The SIMPACK vehicle model exports quantities, such as vehicle speed, yaw angular velocity of the leading bogie or the vehicle position in the track. These quantities will be analysed to obtain the track curvature and generate the reference displacement for each actuator, which is fully described as the active steering schemes in Section 2.3. Then the reference displacement is sent into the actuator model. Each actuator model generates an actuator force and in total eight actuator forces will be sent back into the SIMPACK model. In this way, the active steered vehicle model is integrated.

2.3 Control schemes for active steering

2.3.1 Introduction

The design of control schemes for active steering is a crucial problem that directly decides the complexity of sensors, controllers and steering effects. The control schemes involve two issues:

i) the control principle;

ii) the estimation of track curvature.

Regarding the control principle, two main control schemes have been proposed. Perfect steering [15,16] aims at nulling the longitudinal creep forces on the two wheels in the same axle if no traction or braking force is applied. At the same time, the lateral creep forces on two wheels should be equalised. However, in real operation, direct measurements of creep forces are very difficult. Therefore, practical implementations of perfect steering are based on measuring or observing other

quantities such as the wheelset lateral position relative to the track, the yaw moment in the primary suspension or the wheelset angle of attack. For more details the reader is referred to [4]. Given the complexity implied by measuring or observing these quantities, other control schemes are usually considered for active steering. Imperfect steering control (radial steering control) does not provide the theoretical optimal solution to the control problem, but still can provide satisfactory improvement of the vehicle curving behaviour compared to a passive vehicle and, more importantly, it is much easier to implement than the perfect steering control [4].

Another important issue is to estimate track curvature in real time. The first solution is to store the track layout information in a database and to use geo-localisation system to localize the vehicle along the track, so that the curvature can be obtained from a look-up table. The other solution is to implement real-time measurements of velocities or angular velocities of car-body or bogie and these data will be processed to compute the track curvature. However, this method introduces a delay due to the position of the on-board sensors and, more importantly, due to the need to low-pass filter of the measured signals, to remove the effect of track defects. In reference [17], measurement is attached on the car-body which has a lag of half distance between bogie pivot for leading bogie. This delay has been reduced by a proposed method. However, this method does not consider the track irregularities which will excite random vibrations of the vehicle.

In this paper, we propose three different control schemes here and study their effectiveness in terms of wheel wear evolution in Section 4.

2.3.2 Three control schemes for active steering

Scheme 1: ‘Radial control + real-time curvature measurement’

Scheme 1 adopts Radial control (imperfect control) and measures the angular velocity of the bogie to obtain the track curvature in real time, which is an easily accomplished scheme in real service. In this control, the radial position of the wheelsets in curves is the control target, as shown in Figure 2, regardless of speed profile and uncompensated lateral acceleration.

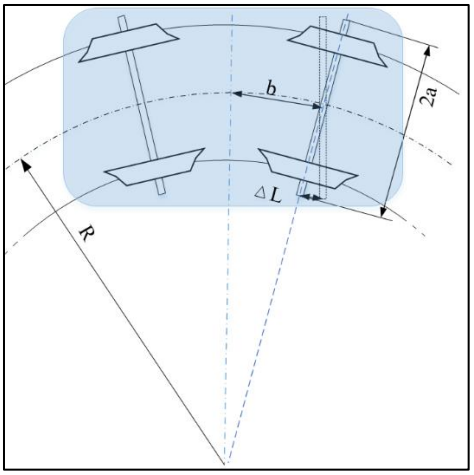

Figure. 2 Radial control scheme

To achieve this, the displacement ΔL of the actuator is controlled. Its reference value can be calculated as:

$$\Delta L_{ref} = \frac{b}{R} \cdot a \quad , \tag{1}$$

where b represents the half wheelbase, and a is the half distance between the right and left actuators. The longitudinal speed of the vehicle V and the absolute yaw angular velocity of the bogie (yaw rate) $\dot{\sigma}$ are measured to calculate the track curvature

$$1/R = \frac{\dot{\sigma}}{V}. \tag{2}$$

More information for this method can be referred in reference [14].

Since the track irregularity causes noise of the measured signals of V and $\dot{\sigma}$, a low-pass filter is introduced to extract the real track layout information, but this will cause a time delay when a vehicle enters a curve transition. To alleviate the effect of this delay, a precedence control method, that has been widely implemented in tilting trains [2,18], is adopted in which the signal measured at the front of the vehicle is delayed by a proper amount of time considering vehicle speed and distance between wheel axles. Then the delay caused by the low-pass filter can be compensated for the following wheelsets. Unfortunately, this method is inherently not capable of compensating delays in the leading wheelset of the vehicle.

Scheme 2: 'Radial control + Geo-localisation system'

To solve the problem of track curvature estimation delay in Scheme 1, Scheme 2 applies the track layout database and geo-localisation system to obtain the track information. The error of this

method mainly comes from the tolerance of the geo-localisation system, but technologies like Kalman filter can be used to merge information from different channels for instance from speed profile, GPS signal and odometry to improve the accuracy of vehicle localisation [19,20]. This error could thus be controlled to a small value and in this study the accurate position of the leading wheelset along the track is obtained from the multi-body simulation model. Figure 3(a) compares the curvatures obtained via Scheme 1 and Scheme 2 in curve R400, where Scheme 2 presents the accurate track curvature whilst a lag of 0.5 seconds can be noticed for Scheme 1. Figure 3(b) compares the reference displacement of the actuators on the leading and trailing wheelset. The reference displacement generated by Scheme 1 for actuators on the leading wheelset is lagging behind the one from Scheme 2, but with precedent control scheme this lag can be compensated for the trailing wheelsets, see Figure 3(b), where the red dashed line and the red solid line have negligible difference .

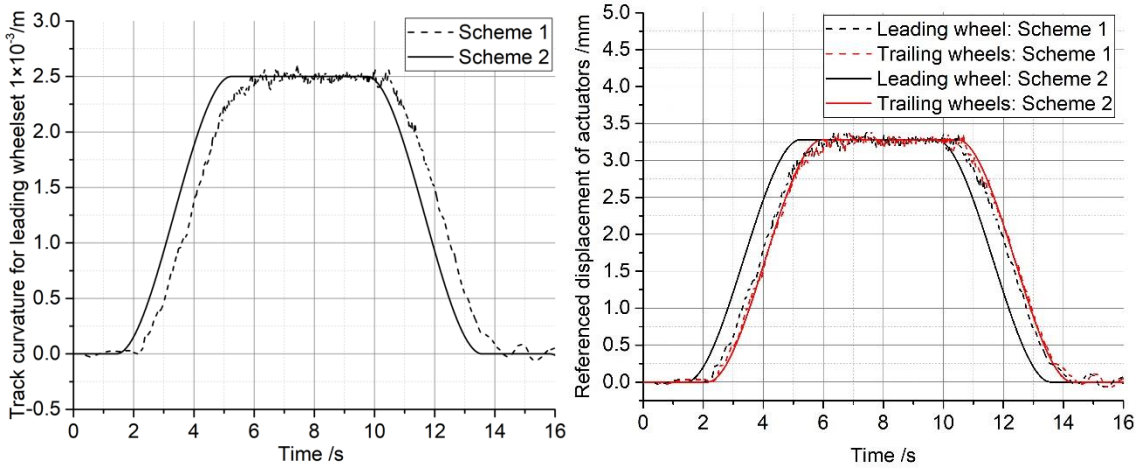

(a) track curvature estimation *(b) reference displacement of actuators*

Figure 3 Comparison of (a) track curvature estimation and (b) reference displacement of actuators between Scheme 1 and Scheme 2

Scheme 3: 'Perfect control'

Scheme 3 applies the so-called perfect control. In the theory of perfect control, the longitudinal creep force of wheels on the same wheelset should be equal or zero if no traction or braking force generated. Therefore the control in Scheme 3 is based on equal longitudinal creep forces of wheels on each wheelset as introduced in reference [10]. Accurate measurement of longitudinal creep forces is still challenging, nevertheless some methodologies have been proposed to estimate these quantities [21]. However, this is not the concern of this paper where we focus on the difference of the perfect control and the radial control in terms of wheel wear. Thus, we directly obtain the accurate longitudinal creep forces from the multi-body simulation model. The difference of

longitudinal creep forces between left and right wheels is used as the feedback signal and a PI controller is applied to generate a control force to equalize the creep forces for both wheels on the same wheelset. The dynamics model of the actuators in this scheme is not considered to form an ideal 'best case' for this control scheme.

The comparison between Scheme 3 and Scheme 2 can help us to understand how much further improvement could be reached applying the perfect control scheme and whether it is worth striving for a more sophisticated active steering system.

The wear numbers of the leading wheelset in curve R400 for the vehicle with passive suspension and the above-mentioned three schemes are compared in Figure 4 (a) and (b) respectively with and without track irregularities.

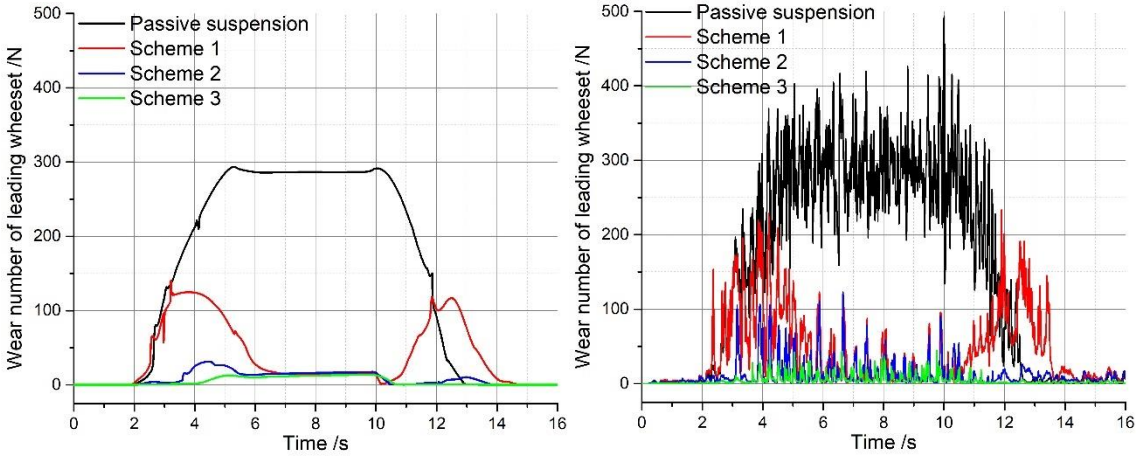

(a) without track irregularities *(b) with track irregularity*

Figure 4 Wear number of leading wheelset with different suspension schemes (a) without track irregularities and (b) with track irregularities

In Figure 4 (a), Scheme 1 significantly improves the wear number in the circular curve but two waves are noticeable at curve transition due to the delay from track curvature measurement. These two waves almost disappear in Scheme 2 where a track database and a geo-localisation system are applied so that the signal delay is basically eliminated. Scheme 3 has the best performance although there is very limited space for further improvement with respect to Scheme 2. The results in Figure 4 (b) lead to the same conclusions but, when track irregularities are applied, the difference between Scheme 2 and Scheme 3 is kind of blurred.

The above analyses lead to an initial understanding of different control schemes for active steering, whilst a detailed investigation is performed in terms of wheel wear evolution in following sections.

3 Wear calculation methods

3.1 Wear model

The wear calculation method follows the 'KTH wear model' which is based on Archard's model and uses a Wear coefficient map [22,23]. This method has been proved reliable to predict the wheel wear and has been compared with other classic wear methods, showing good performance [24–26].

In this work, Hertz contact is applied to calculate wheel-rail normal pressure, and FASTSIM to calculate the shear stress. According to the principle of Archard's model, the wear depth at the wheel surface Δz in the co-ordinate of each contact patch (x, y) is a function of contact pressure p_z and relative sliding distance s between wheel and rail,

$$\Delta z(x, y) = k \frac{p_z(x,y) \cdot s(x,y)}{H} \tag{3}$$

where k is the wear coefficient and H is the hardness of wheel surface. The contact pressure $p_z(x, y)$ and the sliding distance $s(x, y)$ can be obtained through the equations described in references [24,27]. The selection of k follows the Wear coefficient map proposed by KTH based on laboratory tests in dry and clean contact condition. To consider the contamination and moisture between wheel and rail in service, Jendel applied a scaling coefficient (1/5.5) on the wear coefficient to reflect the influence of these factors.

Applying the above-mentioned wear model, two examples of wear at a single contact patch are shown in Figure 5.

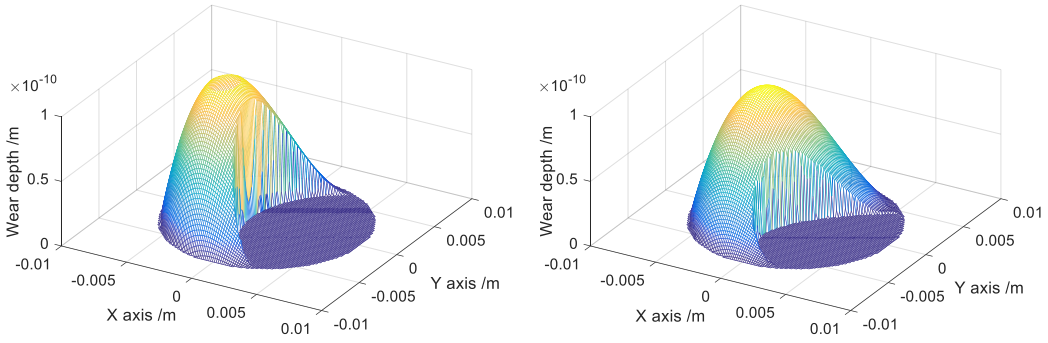

(a) wear with small spin *(b) wear with large spin*

Figure 5 Wear depth within single contact patch with (a) a small spin and (b) a large spin

The wear depth accumulated on the wheel transverse profile for the time of passing distance of one contact patch is the summation of wear depth on each lateral strip from leading edge to trailing edge.

3.2 Wheel profile smoothing and updating strategies

The wheel-rail contact parameters are obtained at different time steps from multibody simulation and the wear inside each contact patch can be calculated according to the method in Section 3.1. To find a balance between accuracy and computational efficiency, not all the wear depths in each time step need to be calculated but only sampled ones in the distance of L_{sample} (m). We adopt half wheel circumference πr_0 for L_{sample} which will have a good agreement to a simulation with smaller L_{sample} [28]. This L_{sample} also doubles the simulated running distance. It is worth mentioning that with evolution of wheel wear, the wheel/rail geometry contact tends to increase conformity in some contact zones like the wheel tread [29]. In SIMPACK, we start with new S1002 / UIC 60 profiles where single-point contact is used in the first few wear steps while multi-point contact will be activated automatically with increasing conformal contact in the following wear steps. In the simulation case for passive suspension, we observe the conformal contact at the wheel flange root with evolution of wheel wear. Therefore, the wear calculation must consider multi-point contact in one single integration step to avoid under-estimation of material removal over the wheel profile in the later stage.

The left and right wheels on the same wheelset will run on the symmetrical left and right curves and we assume that the vehicle runs in both directions. Presumably, for our vehicle model with four wheelsets, the wheels on the leading wheelset and the fourth wheelset have the same wheel profile as 'Outer wheels' whilst the wheels on the second and third wheelsets share the same wheel profile as 'Inner wheels'. The wear calculation for either outer wheels or inner wheels takes contact quantities from four wheel-rail pairs as input which further quadruples the simulated running distance, i.e. saving computing time.

Once accumulated material removal over the wheel profile is computed, smoothing needs to be performed before starting a new iteration to eliminate artificial spikes coming from numerical calculation procedures. A classic smoothing method is applied where the material removal is first filtered by a moving average and afterwards cubic spline smoothing is adopted for the updated wheel profile [30,31]. Regarding the wheel profile update strategies, in each wear step the maximum wear depth Δz_{max} is limited to 0.1mm and the running distance should not exceed 1500km.

3.3 Parameter configuration

For an inter-city vehicle with maximum service speed of 160km/h, the curve radii in service can vary from sharp curves with 250 m radius that can contribute to severe wear on the wheel flange,

to curves with e.g. 3000 m radius that would cause mild wear on the wheel tread. In other words, wear patterns will vary according to the track layout. The effectiveness and economic impact of active wheelset steering may also vary in different running scenarios. Therefore, we propose three track layouts consisting of different proportions of track segments, as shown in Table 1.

Table 1 Three track layouts and their proportions of different curve radii

Track segments	Sharp curve	Small curve		Large curve		Very large curve		Tangent track
	R250	R400	R600	R800	R1000	R1500	R3000	
Track layout1	0.5%	1%	3%	3%	4%	8.5%	20%	60%
Track layout2	1%	2%	6%	6%	8%	14%	18%	45%
Track layout3	2%	4%	12%	12%	16%	14%	10%	30%

Each track layout has eight representative track segments from sharp curve R250 to tangent track. The parameters of Track layout 2 are very similar to a real track for a regional train in Stockholm [22]. Track layout 1 and Track layout 3 are created for comparison with respect to Track layout 2. The proportions of track segments from R250 to R1000 in Track layout 2 are halved respectively to form the data for Track layout 1 and they are doubled for Track layout 3. The tangent track percentage is hence higher for Track layout 1 (60%), intermediate for layout 2 (45%) and lower for layout 3 (30%).The parameters for three track layouts are in a reasonable range for rail networks in reality, whilst two extreme cases with a more curved layout and a less curved layout are referred in [26] and [31] respectively. In this paper, the track gauge widening is not considered.

Each track segment is modelled in one SIMPACK model file where the track configuration starts with a short tangent track followed by a curve transition, the circular curve, another curve transition, tangent track and a symmetrical curve section in opposite direction. The configuration for each track segment can be found in Table 2. In each wear step, the removed material for each track segment is weighted by w_i according to the proportion defined in Table 1 and then is accumulated before smoothing and updating of the wheel profile.

Table 2 Configuration in each track segment

Track segments	Speed (km/h)	Curve trasition (m)	Super-elevation (mm)	Track segments	Speed (km/h)	Curve trasition (m)	Super-elevation (mm)
R250	70	100	150	R1000	110	40	60
R400	80	85	120	R1500	130	30	40
R600	90	60	100	R3000	160	20	20
R800	100	50	80	Tangent track	160	/	/

The wheel-rail friction coefficient is an important parameter in the wear model. A value 0.4 or 0.3 is often selected for wear calculation [32]. However, given that the friction coefficient will vary in service according to temperature, humidity and contamination at the wheel-rail surface, it is reasonable to consider the stochastic feature of this factor [31,33]. Here, a Gaussian distribution with mean value 0.35 and standard deviation 0.05 is introduced to generate a wear friction coefficient for each wear step. The variation of friction coefficient brings stochastic influence on vehicle dynamics so that the wheel-rail contact condition is closer to the real one.

3.4 Case studies for vehicle with passive suspension

In this section, case studies of the vehicle with passive suspension are performed to further explain the wear calculation and to reveal the feature of the wear pattern in different track layouts. Figure 6 plots the removed material after a distance of 4 km in the first wear step in the curve segments R250, R600, R1500 and tangent track before smoothing.

Different wear patterns can be noticed in different curves. In sharp curves, a more severe wear takes place at the wheel flange from -0.04 m to -0.03 m and at the wheel tread from 0.01m to 0.02 m when the opposite wheel is flanging, whilst in large curves and especially on tangent track the wear on the wheel flange and the wheel tread is mild, in a smaller order of magnitude.

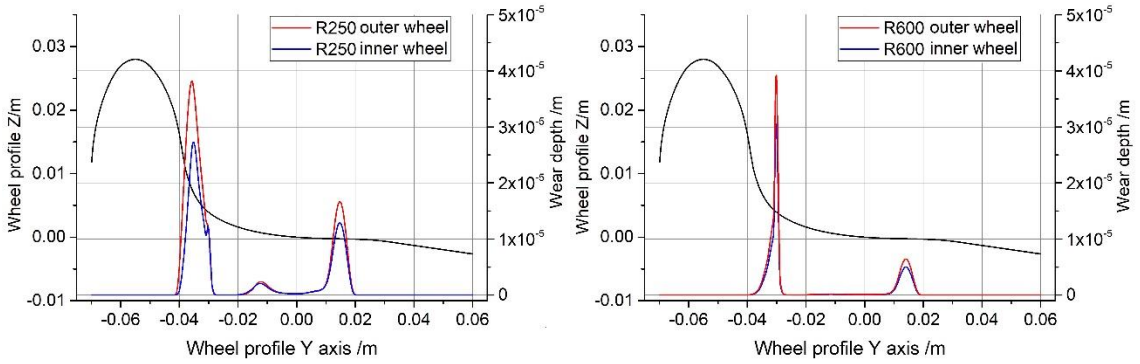

(a) R250 *(b) R600*

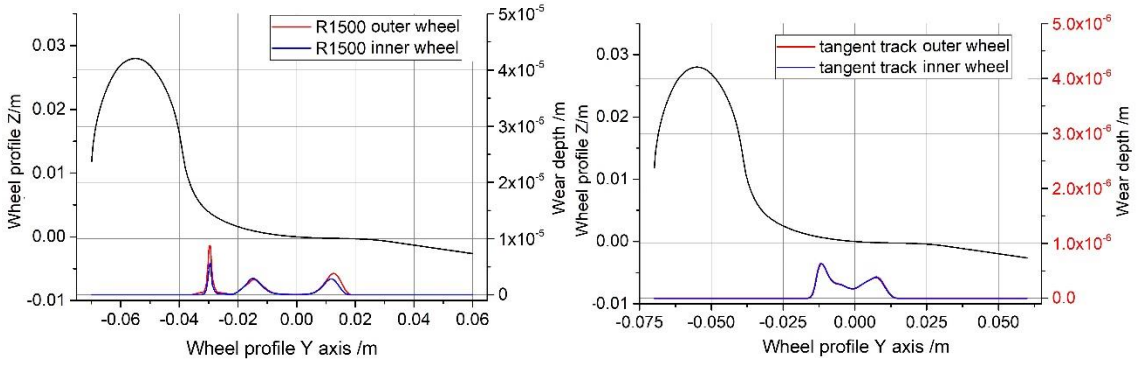

(c) R1500 *(d) tangent track*

Figure 6 Wheel material removal in track segments (a)R250 (b)R600 (c)R1500 (d)tangent track in passive suspension

These results lead us to the fact that the different proportions of track segment in a track layout will cause different wear shapes. Figure 7 compares the material removal of the outer wheel in 3 track layouts after running distance of 50×10^3km and 200×10^3km.

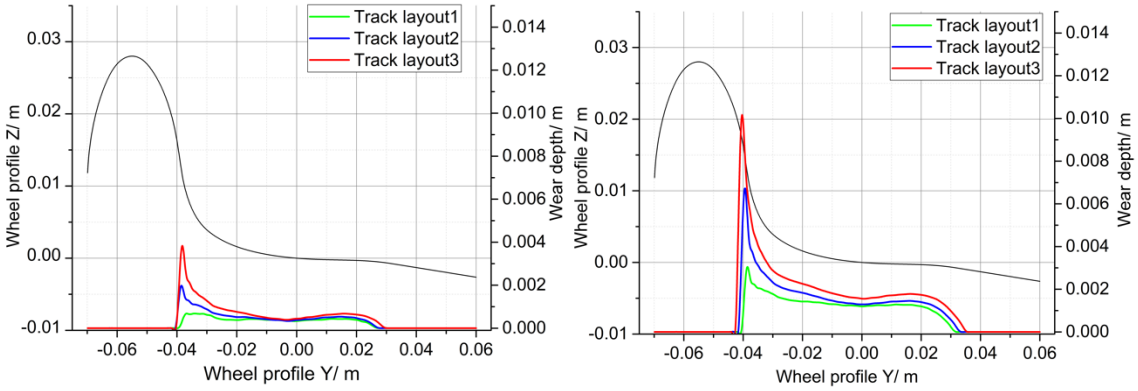

(a) *(b)*

Figure 7 Wheel material removal of outer wheels after mileage of (a) 50×10^3*km and (b)* 200×10^3*km in passive suspension*

According to Figure 7 (a), after the first 50×10^3km operation, the wear taking place on the wheel flange increases from Track layout 1 to Track layout 3 due to the increasing proportions of curves. The wear on the tread develops slowly compared to the wear on the flange. However, the removed material on wheel flange and wheel tread does not increase according to a strictly linear function of the mileage. In the later stage, as is shown in Figure 7 (b), the flange wear on Track layout 3 seems to get slowed down and tread wear increases steadily, although the flange wear is still the dominating wear pattern. The wear on inner wheels shows the same features and is not shown for the sake of brevity. To better understand the wear features in different phases, Figure 8 presents the evolution of flange width S_d.

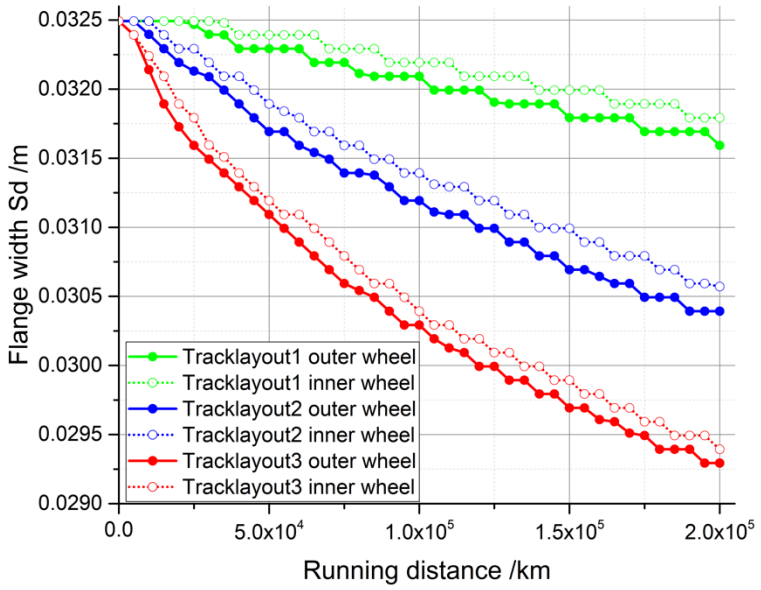

Figure 8 Evolution of flange width S_d in passive suspension

The reduction of the flange width reflects the wear severity at the wheel flange and the curves' gradient in Figure 8 indicates the flange wear rate over running distance. The most severe flange wear happens on Track layout 3 followed by Track layout 2 and 1. Inner wheels show less wear than the outer ones. Besides, the gradients of the curves (especially curves for Track layout 3) tend to decrease with the mileage, showing that the wear distribution either on wheel flange or wheel tread will change in different stages of wheel wear development. The simulations and field tests in References [22,30,34] show the same trend, i.e. that the gradient of the flange width over the mileage is decreasing. Intensive flange wear is observed during the first phase and then the wear rate slows down. This is due to the change of the wheel-rail contact pattern. Conformal contact at wheel flange root is formed in the later stage in our simulation, which leads to less contact at wheel flange in some scenarios. While the wheel flange gets thinner with the progress of wear, the clearance between wheel and rail increases and there are less chances of occurrence of a multipoint contact in small-radius curves, which is the contact condition producing the largest amount of flange wear. However, we should also note that the phenomenon of decreasing flange wear does not always happen, see reference [35] as an example.

Since active steering is dedicated to alleviating wear on curves where flange wear becomes the major wear pattern, we can expect that the effectiveness of active steering might be influenced accordingly in different track layouts and even in different wear phases, which will be verified in the following sections.

4 Wheel wear evolution with active steering

4.1 Comparison and analysis between different control schemes

With the above-mentioned wear calculation method and the introduced three steering schemes in Section 2.3.2, this section studies and compares the steering schemes in terms of wheel wear evolution.

Figure 9 presents the removed material with different steering schemes in Track layout 2 after 50×10^3 km and 200×10^3 km operation. Besides the wear for the vehicle with passive suspension and the three active steering schemes, we also simulate the wheel wear with passive suspension on tangent track, marked as dash-dotted line in the figures. As we know that active steering only works in curves and cannot improve the wear on tangent track, the amount of removed material on tangent track can be used as a reference to show the maximum reduction that active steering could achieve, but there will always be a difference between the 'Tangent track' and the best theoretic steering scheme, due to uncompensated lateral acceleration in curves, resulting in extra tangential and normal forces on wheels.

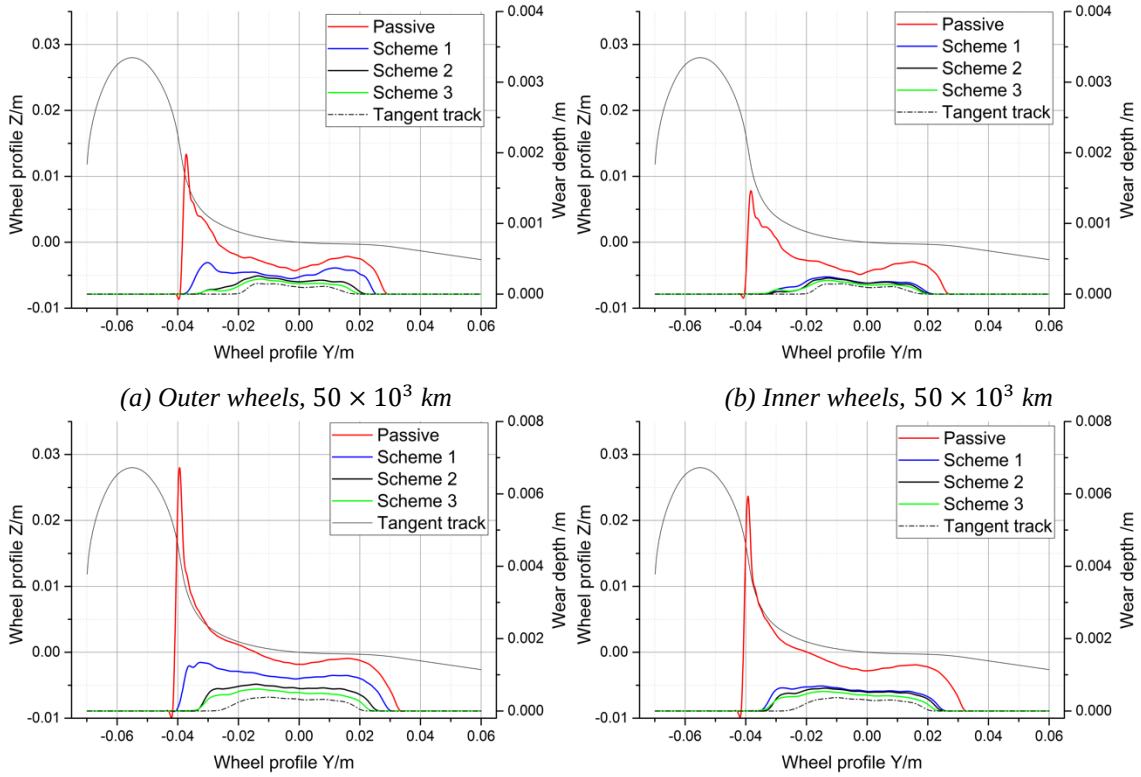

(a) Outer wheels, 50×10^3 *km*

(b) Inner wheels, 50×10^3 *km*

(c) Outer wheels, 200×10^3 *km*

(d) Inner wheels, 200×10^3 *km*

Figure 9 M*aterial removal with different steering schemes in Track layout 2 after* 50×10^3 *km and* 200×10^3 *km operation*

According to Figure 9(a), after the first 50×10^3 km operation, all three active steering schemes provide significant wear reduction at the flange for the outer wheels. The wear with Scheme 2 and Scheme 3 is close to the case of 'Tangent track', showing very satisfactory steering behaviour. However, the difference between Scheme 1 and Scheme 2 is remarkable and reflects the influence of signal delay in curve transition, as introduced in Section 2.3.2. As precedence control is applied, the inner wheels show negligible influence of this time delay so that all the three schemes can produce the desired wear reduction, as shown in Figure 9 (b). After 200×10^3 km mileage, the material removal gets enlarged as well as the space between each line. The features appearing in the first 50×10^3 km still exist in the later stage.

In order to quantify the effectiveness of the steering schemes, we introduce two indicators. The amount of material removal can be expressed as the area below the material removal curve. Based on this, we define the Efficiency E_i of steering Scheme i

$$E_i = \frac{A_i}{A_p} \times 100\% \quad (i = 1,2,3)\,, \tag{4}$$

where A_p is the area of the material removal curve with passive suspension, i.e. the yellow area in Figure 10 (a); $A_i(i = 1,2,3)$ denotes the wear reduction with Scheme 1, Scheme 2, Scheme 3, i.e. the blue area, grey area and green area in Figure 10 (b),(c) and (d).

E_i cannot reach 100% because the wear on tangent track cannot be reduced. It reflects the percentage of wear reduction with respect to the traditional passive vehicle, which can be used as an indicator to show the economic impact of the steering system.

To better compare different steering schemes, we here assume that wear with the perfect steering scheme, i.e. Scheme 3, is 100% satisfactory (nevertheless we later find Scheme 3 is not always the best solution in some situation). Then we define Satisfaction S_i

$$S_i = \frac{E_i}{E_3} \times 100\% \quad (i = 1,2,3) \quad . \tag{5}$$

The Satisfaction S_i can also be understood as efficiency of the steering scheme compared with the theoretically perfect one.

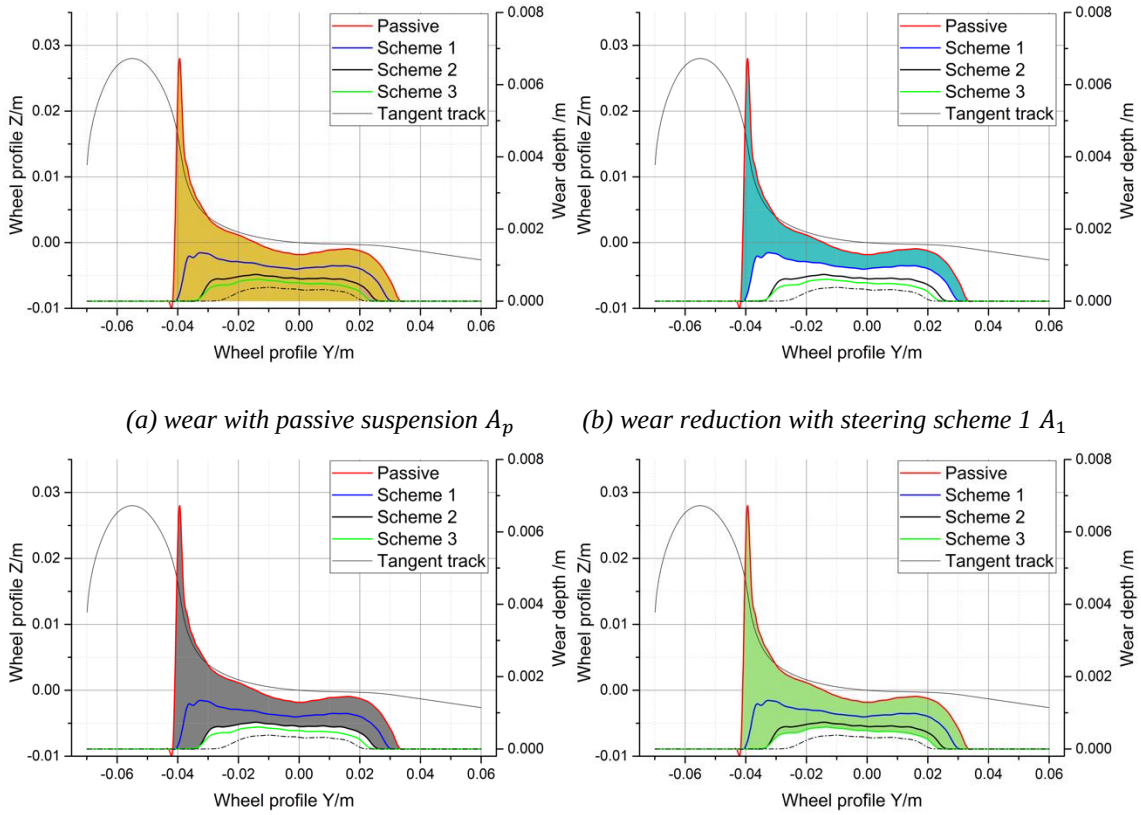

(a) wear with passive suspension A_p

(b) wear reduction with steering scheme 1 A_1

(c) wear reduction with steering scheme 2 A_2

(d) wear reduction with steering scheme 3 A_3

Figure 10 Definition of different terms (a) A_p (b) A_1 (c) A_2 and (d) A_3

Based on the definition of E_i and S_i , we assess the effectiveness of the steering schemes as shown in Figure 11. For the outer wheels, Scheme 1 contributes to 54% wear reduction after 50×10^3 km operation, which is less effective than Schemes 2 and 3, reaching 78% and 83 % respectively. The effectiveness of Scheme 1 on inner wheels increases by 20% compared to the outer ones. For the inner wheels, almost equal-distant improvement can be noticed from Scheme 1 to Scheme 3.

Mileage also slightly affects the effectiveness indicator. With distance increasing from 50×10^3km to 200×10^3, E_i tends to decrease for all schemes. This is due to the variation of the wheel-rail contact and wear pattern in different stages as shown in Figure 8. In the early stage, intensive flange wear occurs on the wheel flange where active steering can play a more important role. However, in the following stage, the flange wear rate slightly decreases and the effectiveness of active steering drops by 5%-3% for Scheme 1 to Scheme 3.

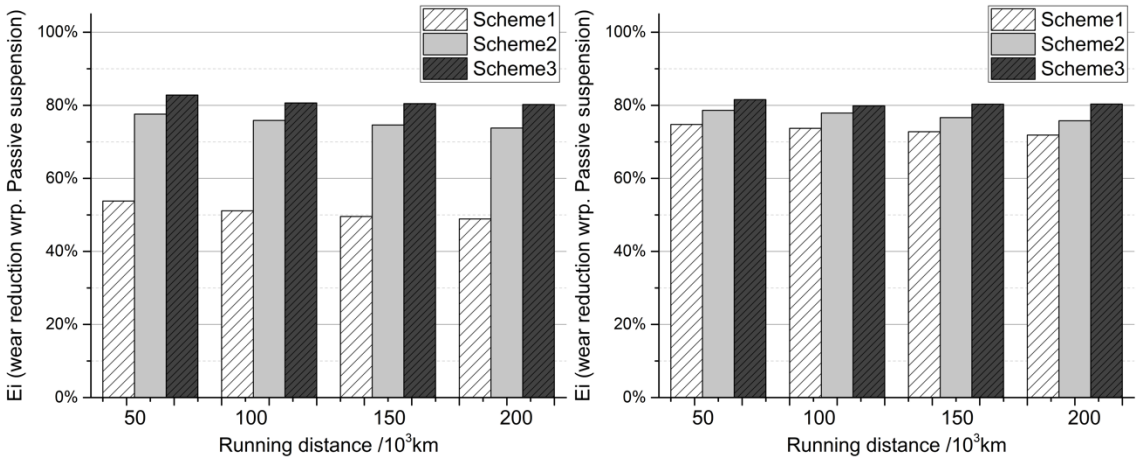

Figure 11 E_i for (a) outer wheels and (b) inner wheels on Track layout 2

Figure 12 summarizes the results for indicator S_i through which we can better compare the three steering schemes. Scheme 3 shows the best performance followed by Scheme 2 and Scheme 1. Scheme 2 is able to provide 91% - 97% efficiency with respect to Scheme 3, from 50×10^3 km to 200×10^3 km mileage. Wheelset steering is more efficient for the inner wheels than for the outer ones. The Satisfaction of scheme 1 varies a lot between outer wheels and inner wheels, with a difference of 30% at most. Nevertheless, we should keep in mind that for a typical trainset consisting of 8 car-bodies and 32 wheelsets, there are only four outer wheels on the front and rear wheelset of the trainset. The inner wheels can still have 89%-92% efficiency with respect to the perfect steering.

With these analyses, we can conclude that when the vehicle operates on Track layout 2, the one featured from a real railway network, wheel material removal can in theory be reduced by 80%-83% with the ideal perfect steering control scheme. However, this perfect scheme is difficult to implement in real service and an error from the estimation of feedback signals would somehow impair its effectiveness. Alternatively, Scheme 2 as a practical solution, is capable of producing 91-97% efficiency with respect to the perfect solution. Therefore, it is a strongly recommended scheme for implementation. Scheme 1 is the simplest solution among the three. It shows ineffectiveness for the outer wheels but still satisfactory performance for the inner wheels. Considering the length of the trainset in which the outer wheels only have a much smaller proportion than the inner ones, Scheme 1 can be regarded as a good compromise between complexity and benefits.

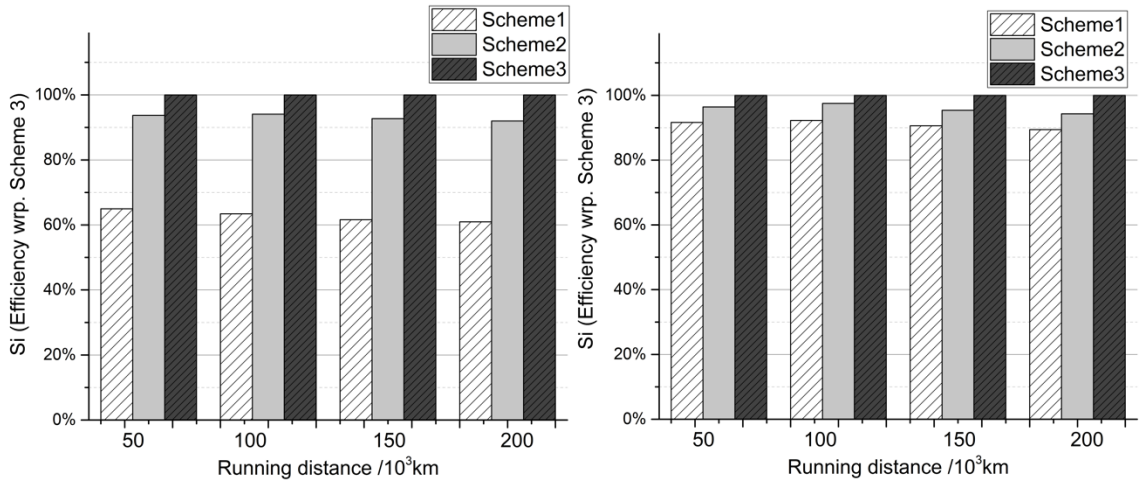

(a) *(b)*

Figure 12 S_i for (a) outer wheels and (b) inner wheels on Track layout 2

4.2 Comparison between different track layouts

As track layouts can affect the wheel wear pattern, the performance of the three steering schemes in three track layouts is analyzed in this Section. Figure 13 compares E_1 (Scheme 1) for the three track layouts. It is clear that effectiveness for both outer wheels and inner wheels will increase from Track layout 1 to Track layout 3 with increasing proportion of curve sections. This can be explained by the wear pattern as well. When the vehicle runs on a more curved track, wheel wear is more likely to appear on the wheel flange where active steering is able to produce more improvement. In other words, the economic impacts of active steering are associated with the amount of curve sections in the track layout. The more curve sections a track layout has, the higher economic impact active steering can produce. The same can be found for Scheme 2 and Scheme 3. For the sake of brevity, all the data for E_i are summarized in Table 3.

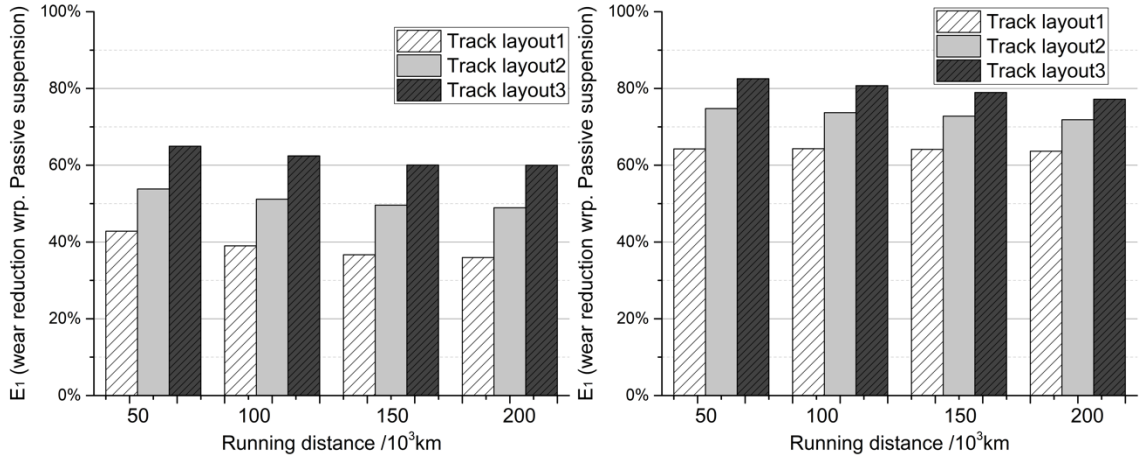

Figure 13 Comparison of E_1 in track layouts for (a) outer wheels and (b) inner wheels

Table 3 E_i of outer wheels in three track layouts and three steering schemes

	Steering scheme 1			Steering scheme 2			Steering scheme 3		
Mileage/km	Track Layout1	Track Layout2	Track Layout3	Track Layout1	Track Layout2	Track Layout3	Track layout1	Track Layout2	Track Layout3
50×10^3	43%	54%	65%	66%	78%	85%	70%	83%	91%
100×10^3	39%	51%	62%	66%	76%	83%	68%	81%	90%
150×10^3	37%	50%	60%	66%	75%	82%	67%	80%	89%
200×10^3	36%	49%	60%	65%	74%	81%	65%	80%	88%

Besides comparing wear reduction with passive suspension, we also compare the schemes in different track layouts through factor S_i. Figure 14 compares S_2(Scheme 2) in different track layouts. When we defined the factor S_i, we assumed that Scheme 3 would be the best steering scheme, and in Section 4.1 we find that Scheme 2 is the best alternative solution to Scheme 3. This is true also for the wear on Track layout 3. However, on Track layout 1 with less small-radius curves and more very large curves and tangent track, the conclusion is different. The value of S_2 increases with the mileage and it even exceeds 100% as shown in Figure 14. In other words, Scheme 2 has better performance than Scheme 3 in the later stage. Figure 15 plots the material removal on Track layout 1 at 200×10^3 km. The green line corresponding to Scheme 3 is slightly above Scheme 2 and the wear zone is also extended. To explain this phenomenon, a deeper study gives that Scheme 3 in the later stage is less effective than Scheme 2 merely in track segment R3000 with maximum speed 160km/h. In this very large curve, the magnitude of the feedback signal for Scheme 3, i.e. the wheel longitudinal creep forces are not as large as the forces in smaller curves. The stochastic track irregularity creates disturbance and it 'destroys' the feedback signal that should have contained clear deterministic track layout information. Simulation tests illustrate that with the removal of track irregularity or decreasing vehicle speed, Scheme 3 regains the best steering effect among the three schemes in curve R3000. Since Track layout 1 has the lowest proportion of small-radius curves and highest proportions of very large curves and tangent track, this ineffectiveness develops with operation mileage in this track layout.

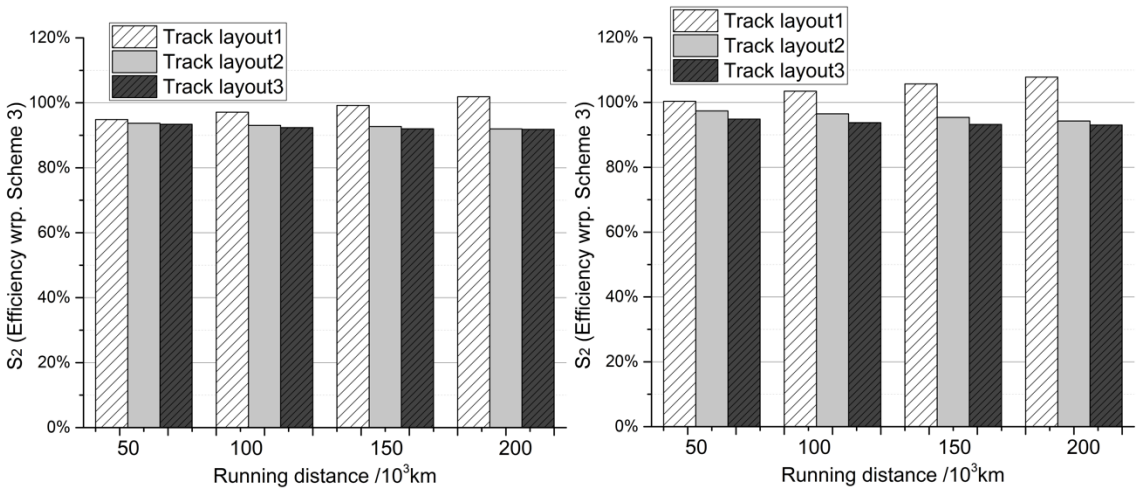

(a) Outer wheels *(b) Inner wheels*

Figure 14 Comparison of S_2 in three track layouts for (a) outer wheels and (b) inner wheels

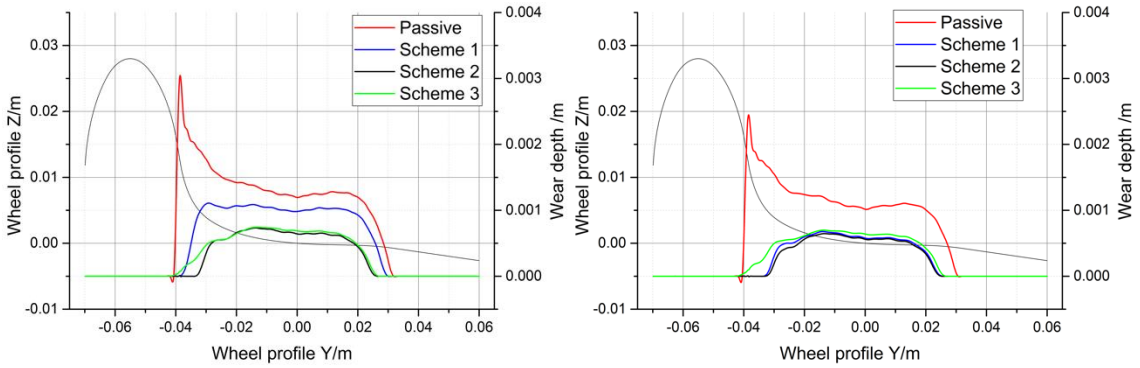

(a) Outer wheels *(b) inner wheels*

Figure 15 Material removal of (a) outer wheels and (b) inner wheels after $200 \times 10^3 km$ mileage

5 Examination on simplified method

Above sections calculate the evolution of wheel profiles to evaluate the effectiveness of active steering through the factors E_i and S_i. This method needs an iterative wear model and requires a large amount of computing resource. We therefore consider here the impact of using 'traditional' indicators such as the frictional power to quantify the reduction of wear under presence of active steering. These indicators have been widely used in previous research, in a way as shown in Figure 4, but so far, no objective evaluation of the accuracy of these simplified methods was provided. Therefore, we compare the simplified methods with the iterative wear calculation method, and we draw conclusions on the applicability of these simplified methods.

Frictional power [W], defined as the summation of products of creep velocities and creep forces, is a commonly used indicator for the severity of wear [36]. The wear number [N], calculated as frictional power over vehicle speed, is the other frequently used measure to estimate wear severity.

In order to consider the influence of track layout parameters, i.e. the proportions of different track segments, we upgrade the calculation method based on the single wear indicator.

Figure 16 presents the time histories of wear frictional power for the leading wheelset with passive suspension and steering Scheme 1, in track segment R400 consisting of symmetrical curves in left and right direction.

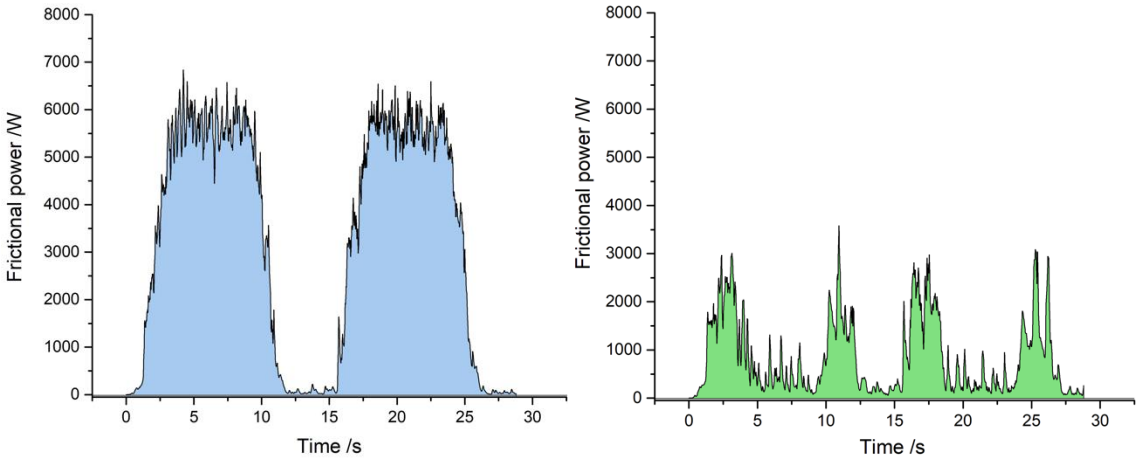

(a) area of Fp in blue *(b) area of $F1$ in green*

Figure 16 The time history of frictional power with (a) passive suspension and (b) active steering Scheme 1

The area under the curve is the total energy dissipated at the contact points, which is related to material removal. The blue area in Figure 16(a), denoted as Fp, corresponds to the material removal with passive suspension and the green area $F1$ in Figure 16(b) represents the material removal with Scheme 1. Unless a proper calibration is performed, it is impossible to derive from these results the actual amount of material that will be removed, but here we are only interested in the ratio between the two cases Fp and $F1$. According to the definition of E_1, the percentage of wear reduction in this single case can be expressed as

$$\widehat{E_1} = \frac{Fp-F1}{Fp} \times 100\% \quad . \tag{6}$$

Considering existence of four wheelsets and eight track segments in our simulation, the complete expression of $\widehat{E_i}$ is defined as

$$\widehat{E_{O,i}} = \frac{\sum_{j=1}^{8} w_j(Fp_{j,1}+Fp_{j,4}) - \sum_{j=1}^{8} w_j(Fi_{j,1}+Fi_{j,4})}{\sum_{j=1}^{8} w_j(Fp_{j,1}+Fp_{j,4})} \quad \text{(i=1,2,3)} \tag{7}$$

and

$$\widehat{E_{I,i}} = \frac{\sum_{j=1}^{8} w_j(Fp_{j,2}+Fp_{j,3}) - \sum_{j=1}^{8} w_j(Fi_{j,2}+Fi_{j,3})}{\sum_{j=1}^{8} w_j(Fp_{j,2}+Fp_{j,3})} \quad \text{(i=1,2,3)} \ , \tag{8}$$

where $\widehat{E_{O,i}}$ and $\widehat{E_{I,i}}$ are factors for the outer and inner wheels respectively with steering Scheme i ; w_j is the weighting coefficient of the jth track segment defined according to the proportions of track segments in Table 1. Fi $(i = 1,2,3)$ represents the area with Scheme i. For $Fp_{j,k}$ and $Fi_{j,k}$, the first

subscript j denotes the number of track segments and the second subscript k varies from 1 to 4 to denote the number of the wheelset.

Once we get the estimation of $\widehat{E_i}$, the $\widehat{S_i}$ can be computed according to Equation (5).

This simplified method is performed with the new wheel and rail profiles and it only has one value regardless of mileage and variation of wheel-rail geometry contact. The calculated $\widehat{E_i}$ based on frictional power and wear number is summarized in Figure 17.

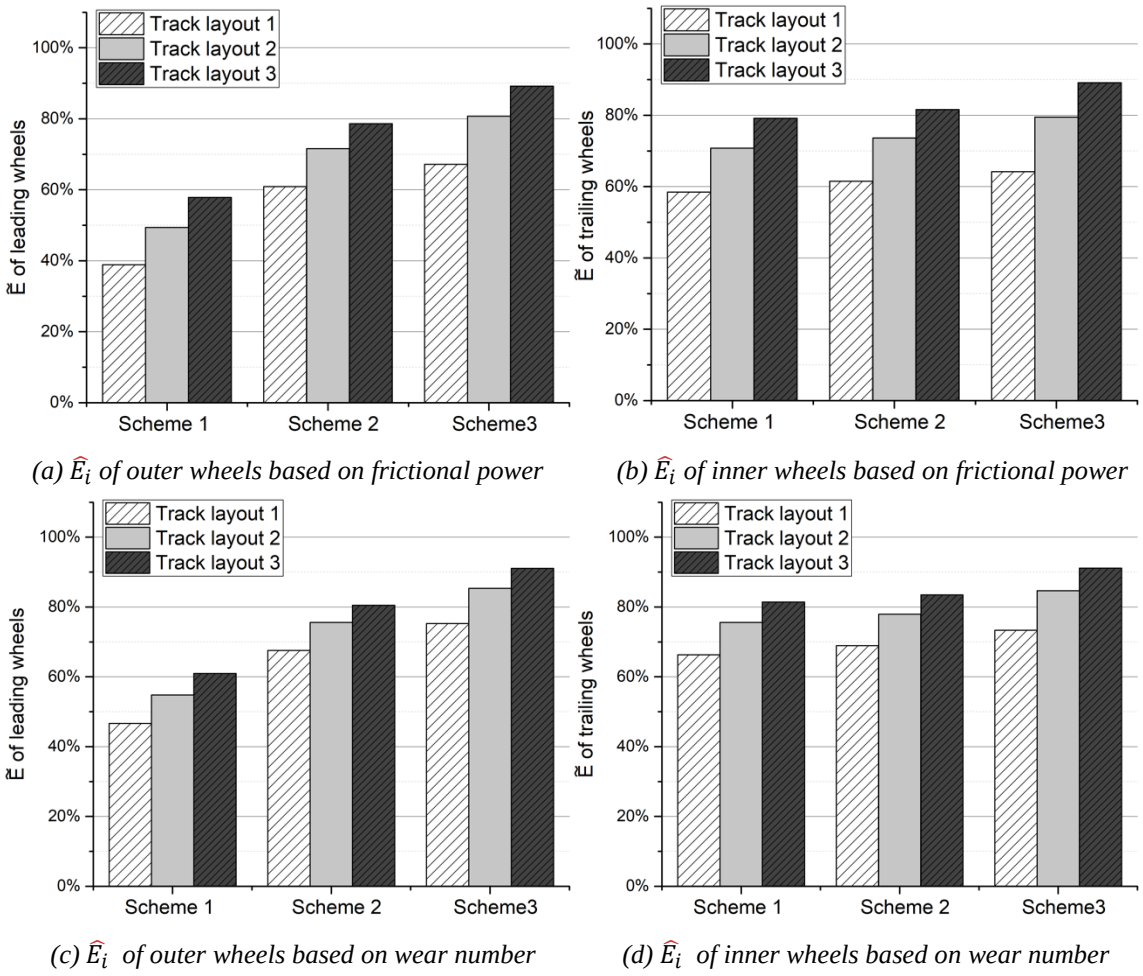

(a) $\widehat{E_i}$ of outer wheels based on frictional power *(b) $\widehat{E_i}$ of inner wheels based on frictional power*

(c) $\widehat{E_i}$ of outer wheels based on wear number *(d) $\widehat{E_i}$ of inner wheels based on wear number*

Figure 17 Estimation of $\widehat{E_i}$ through simplified method.

The estimation of $\widehat{E_i}$ based on either frictional power or wear number presents the same features in the comparison of three steering schemes and different track layouts, as the iterative wear calculation method. Table 4 summarizes the deviation of the simplified method compared to the 'full method' at different mileage. The simplified method based on frictional power gets smaller estimation of $\widehat{E_i}$ than the method based on wear number. The deviation is also decreasing with the mileage because of the decreasing E_i computed by the iterative wear method and the ignorance of evolution of the worn profile in the simplified method.

The errors of simplified method based on frictional power are within 9%, in the mileage of 200×10^3 km on Track layout 2 and the error from the method based on wear number does not exceed 13%. However, these errors will enlarge with the mileage, depending on the extent to which that the wear pattern will change with the mileage.

Table 4 Deviation $((E_i - \widehat{E_i})/E_i)$ of $\widehat{E_i}$ based on simplified method on Track layout 2 (Outer: outer wheels, Inner: inner wheels)

	Method based on frictional power						Method based on wear number					
	Scheme 1		Scheme 2		Scheme 3		Scheme 1		Scheme 2		Scheme 3	
Mileage /km	Outer	Inner	Outer	Inner	Outer	Inner	Outer	Inner	Outer	Inner	Outer	Inner
50×10^3	8.24%	5.29%	7.68%	6.38%	2.50%	2.54%	-1.86%	-1.08%	2.59%	0.87%	-3.03%	-3.80%
100×10^3	3.47%	3.91%	5.58%	5.46%	-0.12%	0.47%	-7.16%	-2.55%	0.37%	-0.10%	-5.80%	-6.00%
150×10^3	0.46%	2.72%	4.00%	3.92%	-0.33%	1.03%	-10.50%	-3.82%	-1.30%	-1.74%	-6.03%	-5.40%
200×10^3	-0.93%	1.46%	2.93%	2.83%	-0.62%	1.06%	-12.04%	-5.17%	-2.43%	-2.90%	-6.34%	-5.37%

Table 5 summarizes the error of $\widehat{S_i}$ with respect to the iterative wear method. The deviation of the estimated indicator $\widehat{S_i}$ is smaller than $\widehat{E_i}$ in general. The method based on frictional power is still a bit better than the one based on wear number, not exceeding 6% within the mileage of 200×10^3 km. From this perspective, the simplified method is applicable to compare different steering schemes. However, the ignorance of wheel profile variation may lead to neglecting some issues, for instance, the drawback of Scheme 3 in Track layout 1.

Table 5 Deviation $((S_i - \widehat{S_i})/S_i)$ of $\widehat{S_i}$ based on simplified method on Track layout 2 (Outer: outer wheels, Inner: inner wheels)

Deviation	Method based on friction power				Method based on wear number			
	Scheme 1		Scheme 2		Scheme 1		Scheme 2	
Mileage /km	Outer	Inner	Outer	Inner	Outer	Inner	Outer	Inner
50×10^3	5.89%	2.82%	5.32%	3.95%	1.14%	2.62%	8.12%	4.50%
100×10^3	3.58%	3.45%	5.69%	5.02%	-1.28%	3.25%	9.14%	5.56%
150×10^3	0.79%	1.71%	4.32%	2.92%	-4.22%	1.50%	7.14%	3.47%
200×10^3	-0.30%	0.40%	3.53%	1.79%	-5.37%	0.20%	6.06%	2.35%

6 Conclusions

In this paper an active wheelset steering system is studied from the perspective of wheel wear evolution. Firstly, a wear calculation code is developed to predict the evolution of wheel wear. Case studies for the passive vehicle reveal the change of wear pattern in different stages. Then, three active steering schemes are proposed. Scheme 1 and Scheme 2 are practical solutions in reality with accessible feedback signals. In contrast, Scheme 3, also called perfect steering, is challenging to implement as it uses the measurement or estimation of longitudinal creep force as feedback signal

which is difficult to obtain with sufficient accuracy. Wear calculation shows that wheel flange wear can be significantly reduced by all steering schemes proposed.

To quantify the effectiveness of steering schemes, a factor E is defined, through which we conclude that approximately 80%-83% of material removal over the wheel profile can be reduced by applying the perfect steering scheme, on a track layout featured from a real railway network. However, the effectiveness E can decrease slowly with increased mileage of the vehicle. Besides, the Satisfaction of steering schemes S is defined to compare different steering schemes. Scheme 2 can generally reach more than 90% efficiency of the perfect control scheme for both outer and inner wheels. Scheme 1 shows ineffectiveness on outer wheels which is caused by the signal delay in curve transition. Nevertheless, the inner wheels still have a satisfactory performance, capable of producing around 90% efficiency. In conclusion, the perfect steering scheme based on longitudinal creep force is not necessary, since Scheme 2 and Scheme 1 are good compromises between steering effectiveness and complexity.

The wear simulations on three track layouts illustrate that the active steering would be more effective if the vehicle runs on a more curved track.

At the end of this paper, the commonly used simplified method is compared with the iteration wear calculation method. The deviation of the simplified method is acceptable in the presented case study, but it may exceed the tolerance with increased mileage cumulated by the vehicle in some other cases.

In addition to summarizing the conclusions, it is necessary to clarify the possible extension and application of this work. The parameters of the vehicle and track layout in this paper are selected to be representative. However, there are some factors, such as the primary longitudinal stiffness, the rail inclination and the track gauge, that can potentially change the wear pattern and affect the effectiveness of steering systems. Although inclusive analyses are not performed for these factors, the methodology has been specified in this paper. When it comes to a real application of active steering, the simulation would be repeated with the specific parameters of the rail and the vehicle. Furthermore, to better quantify the economic impacts of the active steering system in terms of wheel wear, the variation of flange width, equivalent conicity, safety factors such as derailment and bogie lateral acceleration need to be examined so that it is possible to predict the extended wheel re-profiling intervals. Moreover, the wear reduction on rails could also be involved to reveal the potential economic benefit. Besides, a similar study could be performed considering a vehicle with independently-rotating wheels, which would help assessing the benefits (and possible drawbacks)

of this alternative mechanical configuration. These studies are expected to be performed in the future as extensions of this paper.

Disclosure statement

No potential conflict of interest was reported by the authors.

ORCID:

Bin Fu https://orcid.org/0000-0001-5024-4095

Stefano Bruni https://orcid.org/0000-0003-2177-5254

Saeed Hossin Nia https://orcid.org/0000-0002-6346-6620

Sebastian Stichel http://orcid.org/0000-0002-8237-5847

Reference

[1] Goodall RM, Kortum W. Active Controls in Ground Transportation — A Review of the State-of-the-Art and Future Potential. Veh. Syst. Dyn. [Internet]. 1983;12:225–257. Available from: http://www.tandfonline.com/doi/abs/10.1080/00423118308968755.

[2] Goodall R. Active railway suspensions: Implementation status and technological trends. Veh. Syst. Dyn. 1997;28:87–117.

[3] Bruni S, Goodall R, Mei TX, et al. Control and monitoring for railway vehicle dynamics. Veh. Syst. Dyn. [Internet]. 2007;45:743–779. Available from: http://www.tandfonline.com/doi/abs/10.1080/00423110701426690.

[4] Fu B, Giossi RL, Persson R, et al. Active suspension in railway vehicles: a literature survey. Railw. Eng. Sci. [Internet]. 2020; Available from: https://doi.org/10.1007/s40534-020-00207-w.

[5] Fu B, Bruni S. Fault-Tolerant Analysis for Active Steering Actuation System Applied on Conventional Bogie Vehicle. 2020. p. 90–99. Available from: http://link.springer.com/10.1007/978-3-030-38077-9_11.

[6] Research report of Project RUN2RAIL, Deliverable 3.4:Impact assessment. 2019.

[7] Tian S, Luo X, Ren L, et al. Active steering control strategy for rail vehicle based on minimum wear number. Veh. Syst. Dyn. [Internet]. 2020;0:1–26. Available from: https://doi.org/00423114.2020.1743864.

[8] Pérez J, Busturia JM, Goodall RM. Control strategies for active steering of bogie-based railway vehicles. Control Eng. Pract. 2002;10:1005–1012.

[9] Perez J, Stow JM, Iwnicki SD. Application of active steering systems for the reduction of rolling contact fatigue on rails. Veh. Syst. Dyn. 2006;44:730–740.

[10] Farhat N, Ward CP, Goodall RM, et al. The benefits of mechatronically-guided railway vehicles: A multi-body physics simulation study. Mechatronics. 2018;51:115–126.

[11] Park JH, Koh HI, Hur HM, et al. Design and analysis of an active steering bogie for urban trains. J. Mech. Sci. Technol. 2010;24:1353–1362.

[12] Qiao G, Liu G, Shi Z, et al. A review of electromechanical actuators for More/All Electric aircraft systems. Proc. Inst. Mech. Eng. Part C J. Mech. Eng. Sci. 2018;232:4128–4151.

[13] Maré J-C. Aerospace Actuators 1 Needs, Reliability and Hydraulic Power Solutions. Aerosp. Actuators 1. Wiley; 2016.

[14] Fu B, Bruni S. Fault-tolerant design and evaluation for a railway bogie active steering system(submitted to Vehicle System Dynamics, accpeted). 2020;

[15] Iwnicki S, Spiryagin M, Cole C, et al., editors. Handbook of Railway Vehicle Dynamics [Internet]. CRC Press; 2019. Available from: https://www.taylorfrancis.com/books/9780429890635.

[16] Shen S., Mei T. X., Goodall R. M. PJ and HJ. A study of active steering strategies for railway bogie. Veh. Syst. Dyn., vol. 41, no. suppl. 2004. p. 282–291.

[17] Tian S, Luo X, Ren L, et al. Active radial system of railway vehicles based on secondary suspension rotation angle sensing. Veh. Syst. Dyn. 2020;3114.

[18] Persson R, Goodall RM, Sasaki K. Carbody tilting - Technologies and benefits. Veh. Syst. Dyn. 2009;47:949–981.

[19] Albrecht T, Lüddecke K, Zimmermann J. A precise and reliable train positioning system and its use for automation of train operation. IEEE ICIRT 2013 - Proc. IEEE Int. Conf. Intell. Rail Transp. 2013;134–139.

[20] Jiang W, Chen S, Cai B, et al. A multi-sensor positioning method-based train localization system for low density line. IEEE Trans. Veh. Technol. 2018;67:10425–10437.

[21] Ward CP, Goodall RM, Dixon R, et al. Adhesion estimation at the wheel-rail interface using advanced model-based filtering. Veh. Syst. Dyn. 2012;50:1797–1816.

[22] Jendel T. Prediction of wheel profile wear - Comparisons with field measurements. Wear. 2002;253:89–99.

[23] Enblom R, Berg M. Simulation of railway wheel profile development due to wear influence of disc braking and contact environment. Wear. 2005;258:1055–1063.

[24] Enblom R. On Simulation of Uniform Wear and Profile Evolution in the Wheel-Rail Contact.Ph.D.Thesis, Division of Railway Technology, Department of Vehicle Engineering, Royal Institute of Technology (KTH), Stockholm 2006. 2006.

[25] Hossein Nia S, Casanueva C, Stichel S. Prediction of RCF and wear evolution of iron-ore locomotive wheels. Wear [Internet]. 2015;338–339:62–72. Available from: http://dx.doi.org/10.1016/j.wear.2015.05.015.

[26] Pombo J, Ambrósio J, Pereira M, et al. Development of a wear prediction tool for steel railway wheels using three alternative wear functions. Wear. 2011;271:238–245.

[27] Nathan AJ, Scobell A. Rolling Contact Phenomena [Internet]. Jacobson B, Kalker JJ, editors. Foreign Aff. Vienna: Springer Vienna; 2000. Available from: http://link.springer.com/10.1007/978-3-7091-2782-7.

[28] Jendel T. Prediction of wheel profile wear - methodology and verification, Licentiate Thesis, Division of Railway Technology, Department of Vehicle Engineering, Royal Institute of Technology (KTH), Stockholm 2000.

[29] Polach O. On non-linear methods of bogie stability assessment using computer simulations. Proc. Inst. Mech. Eng. Part F J. Rail Rapid Transit. 2006;220:13–27.

[30] Braghin F, Lewis R, Dwyer-Joyce RS, et al. A mathematical model to predict railway wheel profile evolution due to wear. Wear. 2006;261:1253–1264.

[31] Luo R, Shi H, Teng W, et al. Prediction of wheel profile wear and vehicle dynamics evolution considering stochastic parameters for high-speed train. Wear [Internet]. 2017;392–393:126–138. Available from: http://dx.doi.org/10.1016/j.wear.2017.09.019.

[32] Li Y, Ren Z, Enblom R, et al. Wheel wear prediction on a high-speed train in China. Veh. Syst. Dyn. [Internet]. 2019;3114. Available from: https://doi.org/10.1080/00423114.2019.1650941.

[33] Hossein-Nia S, Sichani MS, Stichel S, et al. Wheel life prediction model–an alternative to the FASTSIM algorithm for RCF. Veh. Syst. Dyn. [Internet]. 2018;56:1051–1071. Available from: https://doi.org/10.1080/00423114.2017.1403636.

[34] Muhamedsalih Y, Stow J, Bevan A. Use of railway wheel wear and damage prediction tools to improve maintenance efficiency through the use of economic tyre turning. Proc. Inst. Mech. Eng. Part F J. Rail Rapid Transit [Internet]. 2019;233:103–117. Available from: http://journals.sagepub.com/doi/10.1177/0954409718781127.

[35] Ansari M, Hazrati IA, Esmailzadeh E, et al. Wear rate estimation of train wheels using dynamic simulations and field measurements. Veh. Syst. Dyn. 2008;46:739–759.

[36] Fu B, Bruni S, Luo S. Study on wheel polygonization of a metro vehicle based on polygonal wear simulation. Wear. 2019;